Solid Freeform Fabrication 2017: Proceedings of the 28th Annual International Solid Freeform Fabrication Symposium – An Additive Manufacturing Conference
Reviewed Paper

Thermal History Correlation with Mechanical Properties for Polymer Selective Laser Sintering (SLS)

Samantha Taylor, Joseph Beaman, Scott Fish

The University of Texas at Austin
Mechanical Engineering Department, Cockrell School of Engineering
Austin, TX

Abstract

This study investigates the in-situ monitoring of the Selective Laser Sintering (SLS) process by focusing on finding correlations between tensile strength, elongation to break, and fracture location to the observed thermal history of manufactured parts. It compared the monitoring ability of a stationary reference mid-wave infrared and a bore-sighted mid-wave infrared camera. ZYX tensile bars were built to leverage the high dependence of tensile strength on interlayer bonding, which is generally assumed to be related to layerwise thermal conditions. Various thermal history analysis methods, for example: cold subregion temperature, average layer temperature, and outline average temperature were tested. Additionally, several smoothing techniques that reduced noise over time were assessed for their ability to improve the correlation for each individual method. Overall, cold subregions observed over four layers in a tensile bar's thermal history had the best correlation with fracture location and mechanical strength.

Background

The selective laser sintering (SLS) process was developed at the University of Texas at Austin in the 1980's [1]. In the SLS process parts are formed by layers, about 100 microns thick, of powder being sintered together to form a 3D part. For polymers, the key to the process is to hold the temperature of the powder bed above the glass transition temperature of the material. This prevents the polymer from re-crystalizing and allowing successive layers to be properly bonded together. The thermal state of the powder bed is key in developing desired material properties.

As with all additive manufacturing processes, the layerwise creation of the part can produce anisotropic part properties. In the SLS process, the strength of a part perpendicular to the layer stratification is often weakest because of the interlayer bonds [2]. In this experiment, the parts will be built with the longest dimension of the specimen, which will also be the direction of loading, being along the Z axis which is perpendicular to the layer stratification in order to focus on the strength of the interlayer bonds. The strength of the interlayer bonds is strongly dependent on the thermal state of the layer as mentioned in Bourell et. al [2].

For monitoring the thermal state of a build, the most common method in commercial SLS machines is a single point measurement of the entire build surface. This single point measurement is then mapped to correspond to specific regions of the build surface in order to control the multiple radiation based heaters that perform the finer thermal control of the build surface. In literature, the most common method for monitoring the thermal state of a build in a lab setting is infrared (IR) thermography. Most work has been done with thermal monitoring of the Direct Metal Laser Sintering (DMLS) process. As seen in Krauss et. al., an IR camera was mounted outside the

machine to monitor the temperature of each layer to check the quality of the build [3]. Others have directly monitored the thermal state of the melt pool using various sensors such as a pyrometer and pieced the data together to get an overall image of a part for each layer as seen in Buls et. al. [4]. For this experiment, two mid-wave infrared (MWIR) cameras were used to monitor the build process and will be described further in the experimental setup. A specialized research machine, which is unique to University of Texas at Austin (UT Austin) and will be described in greater detail in the following section, was used to enable the two camera protocol.

The mid-wave cameras do not risk being damaged or influenced by the CO_2 laser wavelength of 10.6 microns due to the cameras only measuring in the 3-5 micron range [5]. One major benefit of the MWIR cameras is that they can achieve faster frame rates which is employed in this experiment with the bore-sighted camera. Another benefit the MWIR cameras is that they can have better temperature sensitivity [6]. This is key in discovering small temperature gradients, which will be necessary for the focus of the data analysis.

Experimental Setup

The SLS builds for this experiment were conducted using the Laser Additive Manufacturing Pilot System (LAMPS). This system is unique to the University of Texas at Austin and will be discussed in this section. More in depth descriptions of all aspects of the machine can be found in Wroe et. al. [7].

LAMPS Machine

The Laser Additive Manufacturing Pilot System (LAMPS) is a custom built research SLS machine that enables the monitoring and control of virtually every process parameter during a build process. For monitoring, the machine has over 40 thermocouples, an Edmund Optic Monochrome USB camera (visual camera) with a frame rate of 25 Hz [8], a FLIR 6701 MWIR camera with a stationary reference frame (stationary reference camera) and a frame rate of 30 Hz [5], and a bore-sighted FLIR SC8243 MWIR camera (bore-sighted camera) with a frame rate of 2.24 kHz [9]. A visual representation of this machine and a cross section view with the camera locations indicated can be found in Figure 1.

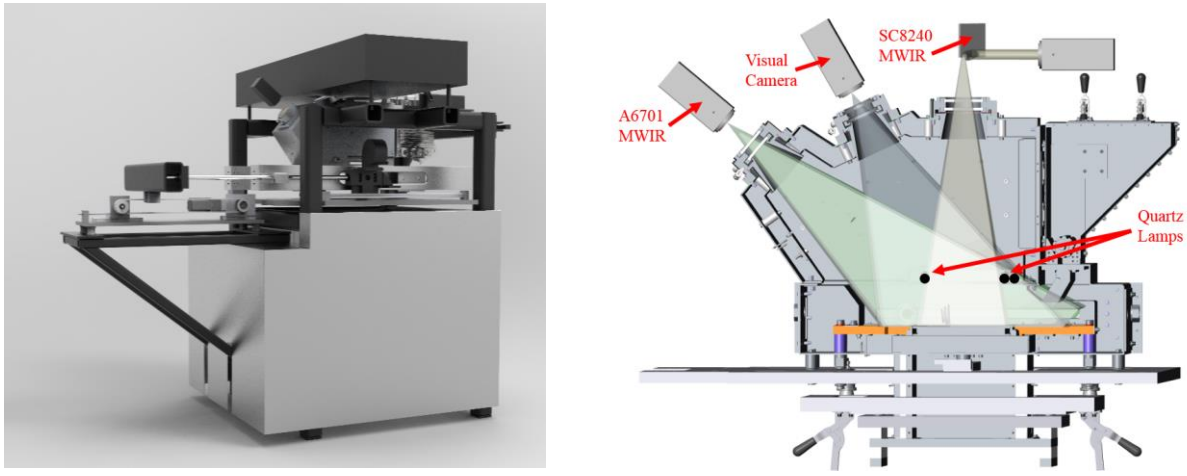

Figure 1: (LEFT) LAMPS Machine (RIGHT) LAMPS Cross Section View; All cameras with field of views highlighted

The LAMPS machine employs the use of a dichroic mirror placed in the optical track of the laser in order to bore-sight the 2.24 kHz FLIR SC8243 MWIR camera with the laser. The dichroic mirror allows for both the laser and the SC8243 MWIR's camera field of view to both travel through the galvanometers, allowing for the camera's images to always be aligned about the moving laser spot. In Figure 2, all the optical track components described are identified.

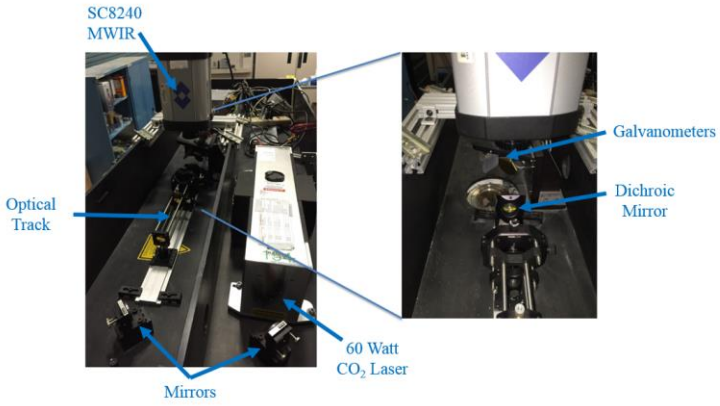

Figure 2: LAMPS Optical Track with highlighted components

Build Setup

Two builds were conducted for this experiment. Each build consisted of 30 tensile bars arranged in a 3 row, 10 column array with the longest dimension of the bars along the Z axis. The tensile bar specimens were similar to ASTM Type A but with a length of 72 mm, a gage section length of 21 mm, and a thickness of 4 mm. The builds were positioned towards one side of the build chamber to prevent the quartz lamp from obscuring the field of view of the stationary reference camera, as can be seen in Figure 3. The quartz lamp with its heat shield atop it can be seen crossing above the tensile bar array in the middle of the image. The heat shield prevents the quartz lamp's radiation from saturating the camera's sensor.

Both builds were conducted with the same lot of Nylon 12 PA 650 powder from Advanced Laser Materials (ALM). All machine parameters were held constant between the builds, except for the set point for the quartz lamps that control the build surface temperature was raised one degree for the second build due to curling issues seen in the beginning of the build. For both builds, the two MWIR cameras' images were recorded throughout the entire gage section of the tensile specimens. The stationary reference camera's images are 512x640 pixels and are taken at a frame rate of 30 Hz. The bore-sighted camera's images are 64x64 pixels and are taken at a frame rate of 2.2 kHz. An example of each camera's image can be seen in Figure 3. The bore-sighted image, seen in Figure 3, has two tensile bar cross sections in its field of view. The laser spot location in the image is indicated while it is in the middle of sintering a single scan line.

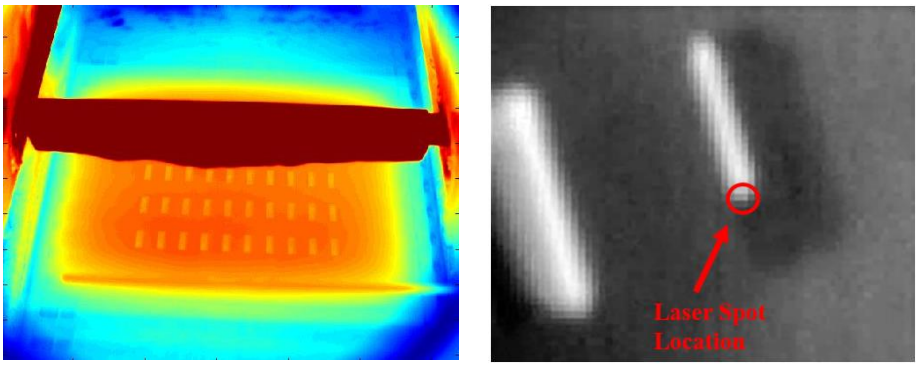

Figure 3: (LEFT) Image taken from Stationary Reference MWIR Camera (RIGHT) Image Taken from Bore-sighted MWIR Camera

The scan strategy employed for both builds was completing all the fill scans for all parts and then perform all the outline scans for each part. The fill scan strategy alternated between layers. For the even layers, all fill scan lines were parallel to the Y axis, or vertical as viewed in the left side of Figure 4. The odd layers had fill scan lines parallel to the X axis, or horizontal as viewed in the right side of Figure 4. The scan line continues along a single coordinate for all bars along that coordinate. Therefore, for the even layers, each column was sintered at the same time, and for the odd layers, each row was sintered at the same time. This scan strategy was implemented in the LAMPS machine as it is a common practice in commercial manufacturers.

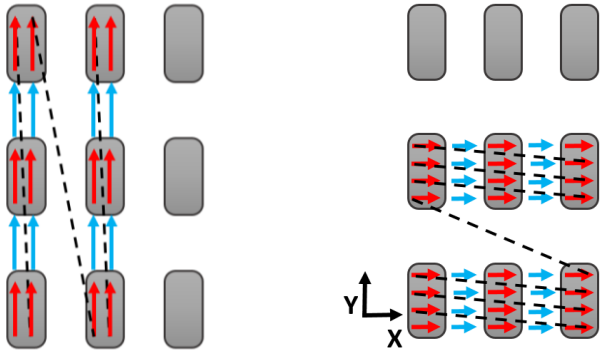

Figure 4: (LEFT) Y axis or Vertical Scan Line Strategy (RIGHT) X Axis or Horizontal Scan Line Strategy

Tensile Test Methodology

Once each build was completed, the specimens were tensile tested according to ASTM 638 methodology with an Instron 3345 testing machine. The stress-strain plot was found for each tensile bar tested. From that plot, the ultimate tensile strength, which was taken as the maximum stress seen during the test, and elongation at break, which was the value of strain at the time of fracture, were found for each tensile bar. To determine exactly where the break of the tensile bar occurred, the total length of the bar was measured before testing and the resultant two parts of the broken bar were measured after tensile testing. The lengths of each half were converted to a layer number using the average layer thickness which was around 3.9 thousandths of an inch. Due to the slight plastic deformation seen by the bars and the fact that not all fracture surfaces occurred within a single layer, there is a range of uncertainty for the exact fracture layer. This error bar range was calculated using the phenomena above, which totaled to +/- 30 layers. If a break location was chosen at random, the probability that if would fall within the error bar surrounding the actual failure location would be about 27%.

Post-Build Analysis

The images collected during both builds from the stationary reference camera and bore-sighted camera totaled over 1.5 TB of data. This data however was reduced through analysis to filter the data down to about 1 GB of data that was used in the final thermal correlations. For the filtering process, different schemes were used for each camera's images in order to select the final data for each tensile bar. The main goal of this initial data analysis was to pick out from the images of each camera a pre-sintered image of each bar and a post-sintered image of each bar. The post-sintered image of each bar for each layer will reveal the quality of the sintered layer through its thermal state. This image will reveal any gradients caused by the laser and quartz lamp heating. It can be seen in the stationary reference image in Figure 3 that the quartz lamp heating can cause significant thermal gradients on the build surface. The reason a pre-sintered image is important is that it has been shown in Philips et. al. that the thermal gradients present in the powder surface pre-sintering are also present post-sintering just at an elevated temperature due to the laser's energy input [10]. Therefore, the post-sintered image and pre-sintered images should be nearly identical except for a temperature shift.

Due to the changing emissivity of the powder once it is in its melted state, when imaged, the tensile bars appear colder than the real temperature when the image is taken due to the time lapse of when the post-sintered image is taken and the beginning of the bar was scanned as seen in Figure 5. Figure 5 is a single tensile bar which has been lased using the X-direction scan strategy as seen in Figure 4 with scan lines being vertical and successive passes moving from left to right. The left side of the tensile bar in Figure 5 appears to indicate that it is cooler than the right side and the surrounding powder bed. This is being caused by the changing emissivity when the part is melted then re-solidified. The emissivity of the powder is different from the emissivity of the melt pools as well as the solidified part. The camera's emissivity is set for the powder because the camera is controlling the quartz lamps that heat the powder bed to keep it above its glass transition temperature and be hot enough to prevent curling of parts when lasing occurs. Therefore, the pre-sintered image removes most emissivity differences out of consideration.

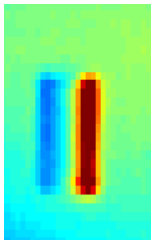

Figure 5: Stationary Reference Camera Post-Sintered Image Zoomed in to One Tensile Bar

Stationary Reference 6701 MWIR Camera Analysis

The stationary reference camera's field of view is of the entire lower half of the chamber of LAMPS machine as can be seen in Figure 3. The camera's image is 512x640 pixels with each pixel's resolution being roughly 300 microns laterally and 650 microns vertically. This camera's primary use is controlling the three quartz lamps that provide the finer temperature control on the build surface. The quartz lamp as mentioned previously provide the higher accuracy thermal control of the powder bed.

Both the pre- and post-sintered images come from single frames from the stationary reference camera due to aliasing caused from the laser's speed of 1.5 m/s being significantly faster than the camera's frame rate of 30 Hz. If several images were gathered and combined to form, for example, the post-sintered image, the number of frames used and the location where sintering occurred would not be consistent from layer to layer or even bar to bar within a single layer. Therefore, only a single frame is used for each the pre- and post-sintered images. In order to find the specific frames used for each of the two images, the location of the laser was tracked. By taking the difference between consecutive image frames, the pixel with largest temperature change corresponds to the laser's current location. Different data filtering schemes were used for the even and odd layers of the build because of the alternating scan strategies between layers seen in Figure 4. For the even layers, which had the vertical scan lines, when the laser's location was about to enter a specific column, that corresponding frame was used for the pre-sintered image for that column of three tensile bars. When the laser spot had just exited a specific column, that corresponding frame was used for the post-sintered image for that column of tensile bars. This same strategy was used for the odd layers but on a row-wise basis instead of column based.

Bore-sighted SC8243 MWIR Camera Analysis

The bore-sighted camera was set up to have a frame rate of 2.24 kHz, with an image size at that frame rate is 64x64 pixels. Each pixel represents an area of around 300x340 microns. As stated before, this camera is bore-sighted with the laser through a dichroic mirror which allows the camera's image to always be centered about the laser spot. Within each layer, the camera is triggered to start recording with a 'begin lasing' signal from the Cambridge EC1000 control board which controls both the laser power and the galvanometer position. When the camera is triggered, it records for a predetermined number of frames, set at the beginning of the build to be able to record the entire duration of the longest layer, which was around 30 seconds of sintering. Therefore, the amount of frames to be recorded was set at 67,000 frames calculated with the maximum frame rate of the camera.

For the post-sintered image of each bar for this camera, individual scan lines were combined together to form an entire cross section for each bar for every layer of the gage section. In order to get to that point the videos taken with the bore-sighted camera had to undergo pre-processing to determine when the laser was firing and which tensile bar it was sintering at the time. For ease of analysis, the pixel value of the laser spot was taken for the entire length of each layer's video and analyzed. Since the post-sintered temperature was being captured, the pixel location chosen was the one that corresponded to the trailing edge of the laser spot. This location was found in the beginning of the analysis process for each build and used throughout the entire analysis for both builds. It was found through a simple simulation that the maximum pixel value in the image represented the trailing edge of the laser spot as seen in Figure 6. The simulation looked at the temperature of a single point in space on the powder bed as the laser scanned over it as it would do during the scanning process in a build. The laser power, speed, and spot size used were those that were measured or input into the machine during the builds. The temperature of the spot was viewed as a function of relative position of the center of the laser spot. When the trailing of the edge of the laser spot was coincidental to the point, the point achieved its maximum temperature. Therefore, this pixel was used for the post-sintered image compilation since it was the point immediately following the laser spot.

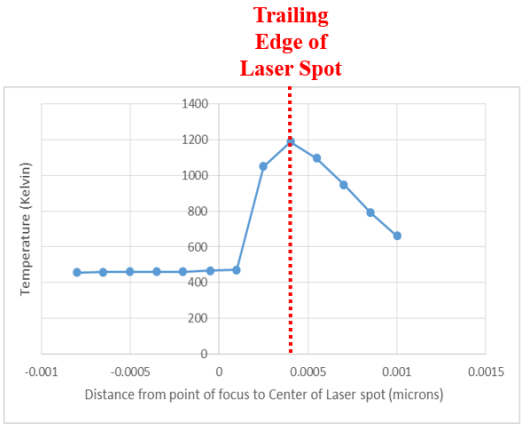

Figure 6: Simulated Thermal Plot Representing Laser Scanning over Powder Bed

The pre-sintered image was found by taking the frame of the bore-sighted video before the laser spot entered each tensile bar's cross section before it was sintered, similar to what was performed with the stationary reference camera's images. The image size of the bore-sighted camera was sufficiently large as can be seen in Figure 3 that the entire area of a single tensile bar was able to be measured in a single frame. The pixel values that represented the tensile bar's cross section were saved for each layer in the gage section.

Thermal Analysis

The methods discussed below were used to perform the thermal analysis for the data retrieved by both the stationary reference and bore-sighted MWIR cameras. A variety of methods were tried, using correlations between the fracture locations of the tensile specimens and tensile strength with certain calculated thermal signatures as a metric for their utility as a future diagnostic tool. Most of the analysis methods focused on the fill scans or inner area of the tensile bars. This was due to the larger volume of data in that area and the ability to filter out that data for both cameras. All methods described below were implemented for both the pre- and post-sintered images gathered by both MWIR cameras.

The fill analysis methods included the average-fill, cold subregion, hot subregion, thermal range, and stacking cold subregion methods. All these methods used the thermal data from the majority of the area of the tensile bar only excluding the outer region of the bar where the outline scan would occur. This thermal data was gathered before the outline scans occurred for each bar in a given layer so as to only account for the thermal contribution of the fill scan lines.

For the average-fill method, the average of the entire fill region of each tensile bar was taken for each layer of the gage section of the tensile bar. Since the bars were built along the Z axis, the interlayer bond strength is what is being tested, and the hypothesis is that the quality of that bond is directly correlated to the thermal state of the layer. Therefore, taking the average of the entire layer would give an indication of the quality of the layer's bond strength. The layer of minimum and maximum of average temperature were then found and its location compared to the break location of the tensile bar. This method worked well for providing a correlation between thermal history and break location as well as strength and will be further discussed later on.

The cold and hot subregion methods had some of the highest correlations between predicted and actual fracture locations of the tensile bars. In looking at the minimum subregion for each layer, it was believed that this region would correspond to a weak area of bonding between layers caused by under-sintering. The hot subregion behavior was also analyzed, but the method did not have a strong correlation with the mechanical properties and will be discussed further in the results section. Looking at the hot subregion in each layer corresponded with the belief that over-sintering an area can also degrade the bond strength by introducing porosity. However, it is believed that the temperatures of the build did not reach this threshold since the difference between the minimum and maximum subregions in a given layer were less than 1 degree Celsius for the majority of the build. Both methods used a moving window of a predetermined size, be it 3x3, 4x4, or 5x5 pixels of the tensile bar's cross section image, which represented a subregion of the bar's cross section for each layer and took an average of each window. A diagram of the method can be seen in Figure 7.

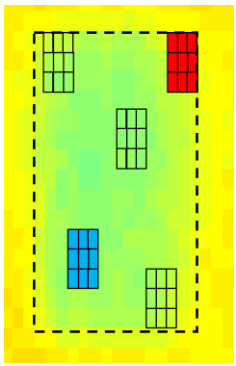

Figure 7: Moving Subregion Method. Pictured is a Single Tensile Bar with 3x3 Pixel Moving Windows with Cold and Hot Subregions Highlighted

The cold and hot subregions were then found by finding the minimum and maximum of the moving windows for each layer. The cold subregion was then analyzed for all layers of the gage section for each bar and the minimum of those cold subregions for the entire gage section was then compared to the break location of the corresponding bar.

The thermal range method that was used leveraged the hot and cold subregion average temperatures. It was believed that physically, the largest difference between minimum and maximum temperatures in a given layer would correspond to larger residual stresses within the build which would cause a weak spot for the tensile bar to fracture. The difference was taken between the hottest and coldest spots in a given layer and then plotted for all layers of the gage section. The layer where this value was greatest was found and compared to the break location of the given tensile bar.

The outline thermal methods included the average-outline and thermal difference method. The average-outline methods took the whole region just where the outline scan occurred and averaged it, and then compared that value over all layers of the gage section. This was done because it has been found that for failure crack initiation can occur due to surface roughness, which would be dictated by the outline scan. The thermal difference method took the difference between the average temperature of the outline scan and the average temperature of the entire fill area of the tensile bar for a single layer and compared that difference over all the layers in the gage section. This method was not as successful as other methods that were implemented.

Smoothing Techniques

For all the thermal methods used, various smoothing techniques were used to enable visibility of trends, noise reduction, and therefore better predictions of break location. Most of the smoothing consisted of taking a moving average of the data in order to filter the data slightly due to the alternating layer scan strategy. Moving average lengths, also described as windows, ranged from 4 to 20 layers. Better predictions came out of smaller windows. For example, a moving average of 4 for the coldest subregion and average of the entire fill area produced the best break location predictions. From looking at the fracture surfaces of the bars, seen in Figure 8, the fracture locations being initiated within a window of 4 layers are confirmed. Since the fractures are very brittle and the layer stratification causes the cracks to propagate near perpendicular to the loading axis, a small moving average window makes sense.

Figure 8: Examples of Fracture Surfaces for Various Tensile Bars

Other smoothing techniques that were employed were due to the alternating scan strategy of the build. Since the thermal state of alternating layers would differ as a result of varying number and direction of scan lines, the various thermal methods (average-fill, cold subregion, hot subregion, etc.) were also analyzed by looking at just even or just odd layers. This technique of looking at only the odd or only the even layers, however was less successful than other methods in fracture location prediction. It is believed that when a cold region is produced in a single layer, that that region can be 'fixed' by the following layer if there is sufficient thermal energy to counteract the cold area. This phenomena, however, cannot be captured when only looking at just the odd or just the even, because it ignores the thermal trends of layers side by side. While this technique reduced noise sufficiently, the moving average described before was the best smoothing technique as it both reduced the noise caused between the alternating layers and smoothed slightly beyond that to produce the best results.

Results

In this section, the best thermal methods, determined by a strong correlation with strength and fracture location, for each IR camera will be the focus of the discussion. Looking at the overall success rates for all the thermal methods, the stationary reference camera had a better ability to predict break locations than the bore-sighted camera. The difference between the two cameras' abilities will be discussed at the end of this section.

Tensile Test Results

For the first build, the average ultimate tensile strength was 39 MPa, and for the second build, the average ultimate tensile strength was 33 MPa. The plot of stress vs strain for each build can be seen in Figure 9 below.

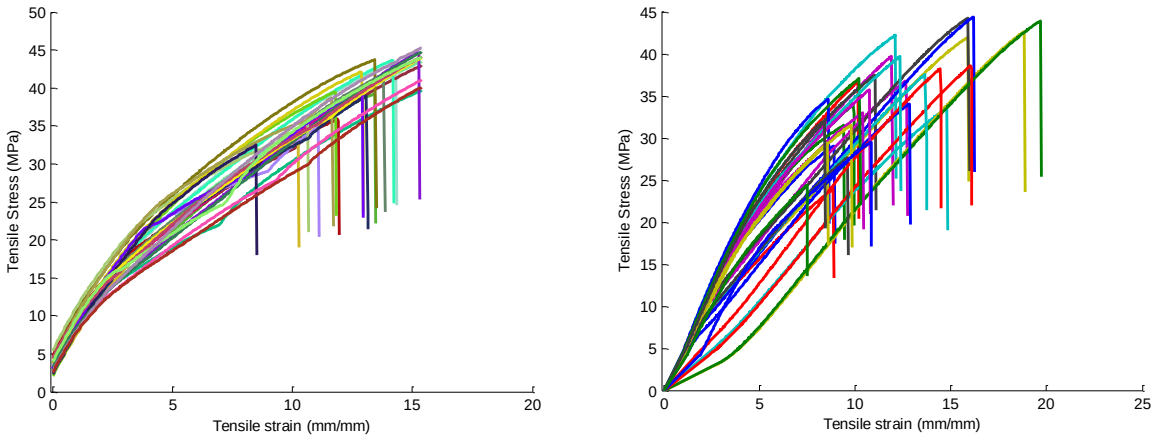

Figure 9: (LEFT) Tensile Results from First Build (RIGHT) Tensile Results from Second Build

Correlation between thermal methods and mechanical properties

In order to validate the ability of a thermal analysis method to correlate with the fracture location of a tensile bar, that method must first have a high correlation with tensile strength to prove that that it highlights a weakness in the tensile bar. Using a combination of the thermal and smoothing techniques that are described above, the single temperature value that was used for the predicted failure location was plotted versus the corresponding tensile strength for each tensile specimen. A best fit line was calculated and the fit coefficient was found. These correlation plots were produced for on the best thermal analysis methods for each build. Examples of the minimum subregion temperature for each build can be seen below in Figure 10.

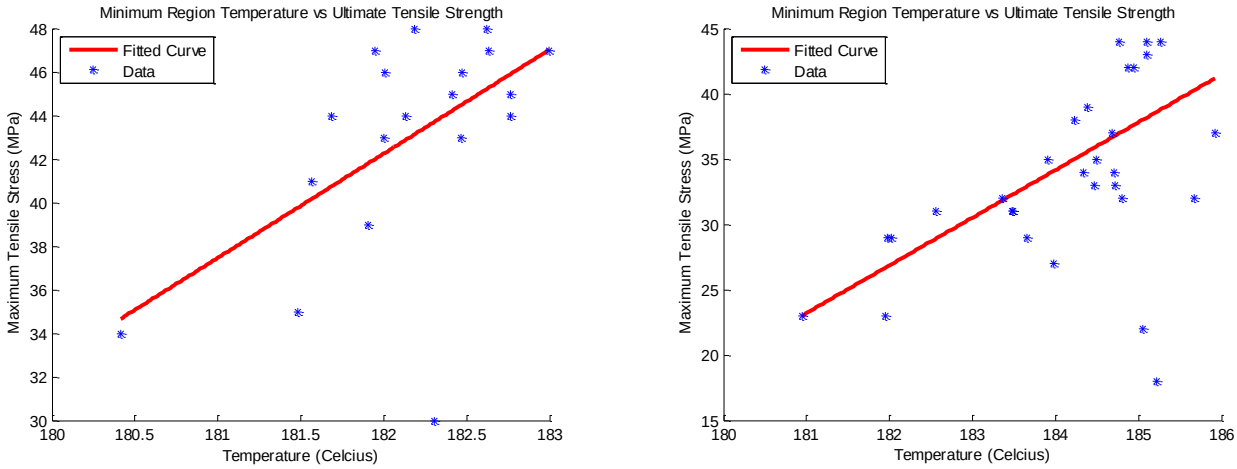

Figure 10: (LEFT) Minimum Temperature Subregion vs Tensile Strength Correlation Plot for the First Build (RIGHT) Minimum Temperature Subregion vs Tensile Strength Correlation Plot for the Second Build

The resultant correlation coefficient for the first build is .59 and for the second build is .55. These correlation coefficients were the highest among the methods, so it is expected that this method would be the best predictor of break location for the tensile bars, because better correlation with strength means that the thermal methods is highlighting the weak points in the bar better.

Best fits were also created using the same failure temperatures but plotted against the elongation at break of the tensile bars to check the strength of this correlation. Examples of this type of plot can be seen below in Figure 11. The correlation coefficients for these plots are .24, for the first build, and .27, for the second build.

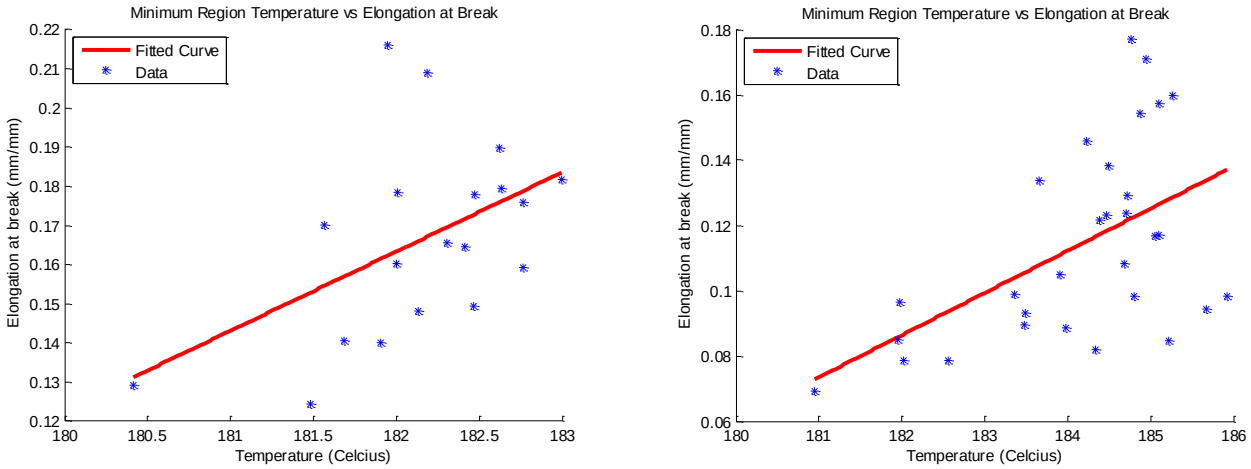

Figure 11: (LEFT) Minimum Temperature Subregion vs Elongation at Break Correlation Plot for the First Build (RIGHT) Minimum Temperature Subregion vs Elongation at Break Correlation Plot for the Second Build

Stationary Reference 6701 MWIR Camera

The best three thermal analysis methods used on the stationary reference camera's images were the minimum subregion, average of the entire layer, and the average temperature of the outline scans. With all the methods, the minimum moving average of 4 layers for each value was chosen as the possible break location for the tensile bar. The pre-sintered images produced better predictions due to the emissivity changes post-sintering and the time scale of when portions of the bar were lased and the post-sintered image were taken as previously discussed. The success rates for each of these methods for both builds can be found in Table 1 below.

Table 1: Stationary Reference Camera Best 3 Thermal Methods' Results

Build	Minimum of Coldest Subregion	Minimum of Average of entire layer	Average of Outline Scan
First Build	45%	45%	35%
Second Build	77%	70%	80%

All of these methods corresponded to weaknesses in the bonding of the layers and would cause weak areas that would allow cracks to initiate and propagate with greater ease. As seen above in Table 1, the best method was the cold subregion, which shows that fracture is dependent on a smaller area than an entire layer. A graph of the best three thermal methods for the gage section can be found in Figure 12. The moving average of 4 layers was implemented to smooth the curves and the absolute minimum layer for each method was found. For the average of the

outline scan, the pre-sintered image was taken after the fill scans were completed. It is believed that this method worked well because the image, due to the time when it was taken, was able to record a more accurate picture of the temperature of the outer area of the tensile bar. This pre-sintered outline image took into account some of the influence of sintering since the outline scan overlaps with some portion of the fill area.

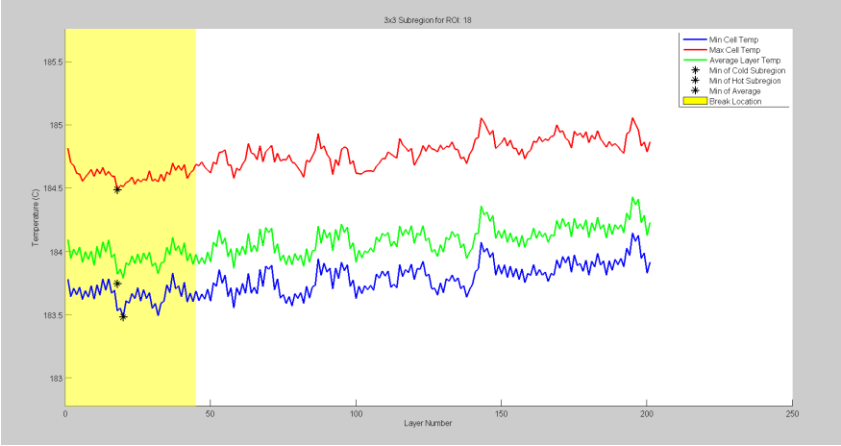

Figure 12: Thermal Plot of Best Three Methods for Gage Section for Tensile Bar 18 in the Second Build

Bore-sighted SC8243 MWIR Camera

For the bore-sighted camera, different thermal methods worked better for each build. The only difference between the builds that was observed is that the quartz lamps, that provide fine temperature control on the powder bed, had set points 1 degree Celsius higher during the second build than the first build. For the first build, the best methods were similar to that of the stationary reference camera. The success rates for this build for the bore-sighted camera can be found in Table 2 below.

Table 2: Best Three Thermal Methods for the First Build with Bore-sighted Camera Measurements

	Min of Coldest Subregion	Min of Average	Min of Hottest Subregion
First Build	43%	43%	43%

The best three methods were finding the minimum of the coldest subregion, average, and hottest subregion of each layer for the tensile bars. An example of the fracture location thermal plots for the gage section for this build can be found in Figure 13 below.

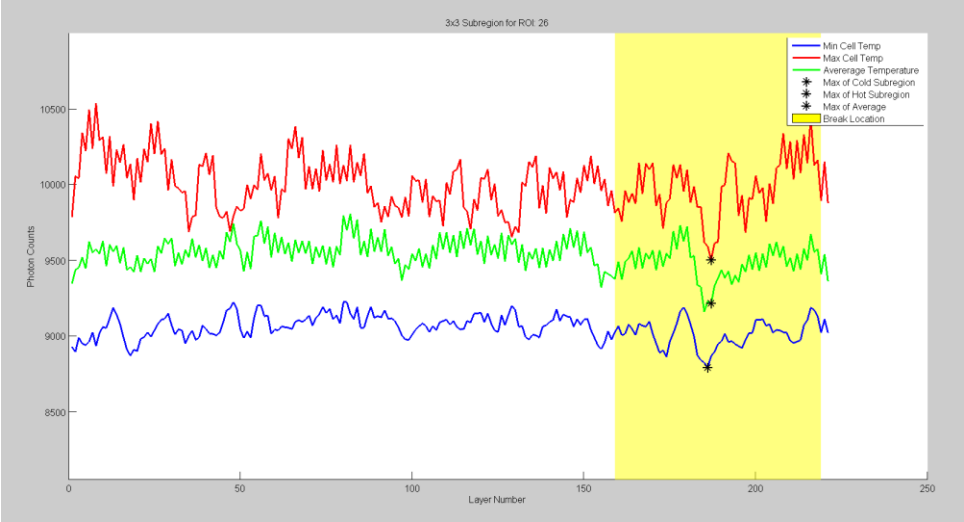

Figure 13: Best Three Thermal Methods for the First Build with Bore-Sighted Camera Measurements

For the second build, the behavior was reversed. The best three methods were finding the maximum of the cold subregion, average, and hot subregions. The success rates for these methods for the November 3 build can be found in Table 3 below. An example of the fracture location thermal plots for the gage section for this build can be found in Figure 14 below.

Table 3: Best Three Thermal Methods for the Second Build with Bore-sighted Camera Measurements

	Max of Coldest Subregion	Max of Average	Max of Hottest Subregion
Second Build	56%	60%	53%

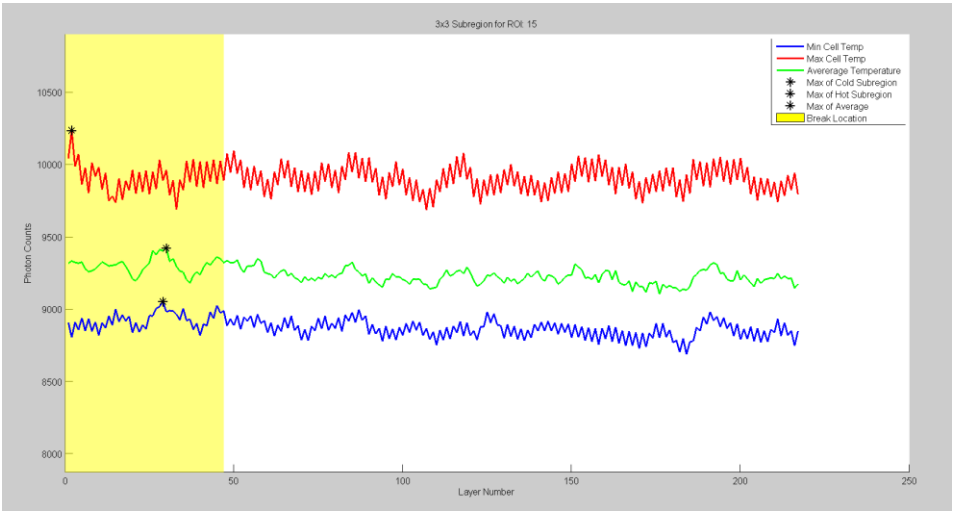

Figure 14: Best Three Thermal Methods for the Second Build with Bore-Sighted Camera Measurements

Although the only difference between the two builds was 1 degree on the build surface, the bore-sighted camera's results changed drastically. The physical reasons behind this change can only be speculated on at this time. It is believed that one possible reason for the change of best

methods is that off gassing produced while each layer is sintered causes reflections and absorption of infrared light that affect the camera's image of the build surface. This could result in the camera viewing a hotspot while on the same location of the build surface actually exists a cold spot [11].

The overall success rates for the bore-sighted camera independent of build or methods, were significantly lower than that of the stationary reference camera. Both cameras are mid-wave IR cameras that should not be influenced by the laser's wavelength. However, the optical trains that the cameras' lines of sight pass through are vastly different. Both camera's line of sight travels through ZnSe windows that allows the infrared light to pass through. That is the only optical object the stationary reference camera's field of view passes through. However, for the bore-sighted camera, its image is reflected by the galvanometer scanning mirrors and dichroic mirror. The laser is also being reflected on these two surfaces as well as traveling through the same ZnSe window that the bore-sighted camera looks through. All three of these surfaces have the ability to heat up due to either direct absorption of the laser's wavelength by the base material of the optical surface or from possible surface contamination that would absorb the laser's wavelength. This heating up of optics would produce a dynamically changing error for the camera [12]. A handheld FLIR E60 long-wave IR camera was used to view the dichroic mirror as the laser scanned the build surface during a single layer. As seen in Figure 15 below, an uneven distribution of the laser's power which can produce variable heating of this optical element is present.

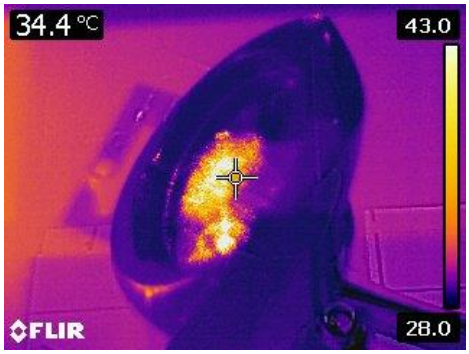

Figure 15: IR Image of Dichroic Mirror during Lasing of Layer

This heating can change over time and cause the dynamic error that would affect the bore-sighted camera's images. This is the most likely cause of the lower success rates of prediction for the boresight camera as the prediction methods are all relative to each tensile bar instead of a set threshold temperature. If there was a constant error that would produce an offset in the camera, it should not affect the camera's ability to find colder regions within the build surface, but since the possible error sources produce a non-uniform heating of optical elements, the camera's images are spatially affected.

Conclusion

Looking at all the thermal methods that were used for both MWIR cameras, the most successful method that predicted the break location of the tensile bars was finding the minimum cold subregion for each tensile bar in the gage section. The size of the subregion needed to be large enough to be able to identify a weak spot with enough size to cause that layer to fracture before other. If the subregion was too small, it did not correlate with the fracture location as well. The cold subregion physically corresponds to a weak spot in the interlayer bonding that would give

way to fracture when under tensile loading. The best subregion was found to be 5x5 pixels in size, which corresponds to an area roughly 1500x3200 microns or 1.5x3.2 mm.

The correlation between the thermal history and the tensile strength of the bars was not as high as expected, given the high success rates of fracture location prediction. The fracture location prediction may have had a higher correlation between the thermal history and the fracture strength because the testing procedure for the tensile bars is affected by human error in the placement of the tensile bar in the testing jaws. This is suggested since each tensile bar was manually loaded into the tensile jaws, the alignment with the long axis of the tensile bar may have been slightly off from the loading axis of the tensile machine. This could allow the loading to not be exactly perpendicular to the layer stratification, which would allow the tensile strength to not solely depend on the interlayer bond strength, which was the assumption of this study. Another reason for the poorer correlation with tensile strength is that differences in minimum temperature between bars can be as low as tenths of a degree Celsius, which is well within the error range of the cameras which is +/- 2 degrees C [5].

When viewing the fracture location prediction success rates between the two cameras, it is clear that the optical track of a given camera effects the results significantly. Even though the stationary reference camera only had a frame rate of 30 Hz compared to the bore-sighted camera with its frame rate of 2.24 kHz, it was the more successful camera, which demonstrates that high speed monitoring is not necessary if looking at the overall quality of a layer. It may be needed for more specific monitoring such as with the melt pool. However, for layer bond strength, an overall image is needed, rather than images of individual scan lines. The pre-sintering image thermal data had a higher correlation with mechanical properties than the post-sintering image thermal data. After sintering occurred, the emissivity of the bar is not consistent, as some portions are still liquid with a lower emissivity than the powder emissivity that is input into the camera, and therefore would affect the measurements. Since measuring the temperature of the bars immediately following sintering is complicated by the variable emissivity, a period of time needs to elapse before measurements can be taken where the emissivity is near constant throughout the tensile bar. In using the either the pre- or post-sintered images, the need for high speed cameras diminishes, as a single image can be used for the pre-sintered image for either camera versus the post-sintered image had to be pieced together from several images with the bore-sighted camera. This allows for a smaller storage of data, which when the need for keeping all data from builds as a quality check will decline the need for larger storage servers.

References

[1] U. o. T. a. Austin, "Selective Laser Sintering, Birth of an Industry," 6 December 2012. [Online]. Available: http://www.me.utexas.edu/news/news/selective-laser-sintering-birth-of-an-industry. [Accessed 2017].

[2] D. L. Bourell, T. J. Watt, D. K. Leigh and B. Fulcher, "Performance Limitations in Polymer Laser Sintering," *Physics Procedia*, pp. 147-156, 2014.

[3] H. Krauss, C. Eschey and M. F. Zaeh, "Thermography for Monitoring the Selective Laser Melting Process," in *Solid Freeform Fabrication Symposium*, Austin, TX, 2012.

[4] S. Buls, S. Clijsters and J.-P. Kruth, "Homogenizing the melt pool intensity distribution in the SLM process through system identification and feedback control," in *Solid Freeform Fabrication Symposium*, Austin, TX, 2014.

[5] FLIR, "FLIR A6700sc MWIR Datasheet," 2017. [Online]. Available: http://www.flir.com/science/display/?id=67022.

[6] Optotherm Thermal Imaging, "Camera Components Infrasight IS640 Radiometric Infrared Camera Competitive Advantages," 2017. [Online]. Available: http://www.optotherm.com/camera-advantages.htm.

[7] W. W. Wroe, "Improvements and effects of thermal history on mechanical properties for polymer selective laser sintering (SLS)," 2015 August 2015. [Online]. Available: https://repositories.lib.utexas.edu/handle/2152/31997?show=full.

[8] Edmund Optics Inc., "EO-1312M ½" CMOS Monochrome USB Camera," 2017. [Online]. Available: https://www.edmundoptics.com/cameras/usb-cameras/eo-usb-2-0-cmos-machine-vision-cameras/59365/.

[9] FLIR Systems, Inc., SC8240 User's Manual, Nashua, NH: FLIR Systems, Inc., 2013.

[10] T. Phillips, A. McElroy, S. Fish and J. Beaman, "In-Situ Laser Control Method for Polymer Selective Laser Sintering (SLS)," in *Solid Freeform Fabrication Symposium*, Austin, TX, 2016.

[11] M. Benedict, Interviewee, *Senior Materials Engineer, Materials & Manufacturing Directorate, AFRL*. [Interview]. 22 February 2017.

[12] D. T. Milner, Interviewee, *Dynamic Errors in Infrared Optics.* [Interview]. 16 February 2017.